
Detecting Spurious Correlations with Sanity Tests for Artificial Intelligence Guided Radiology Systems

Usman Mahmood^{1,*}, Robik Shrestha², David D.B. Bates³, Lorenzo Mannelli⁴, Giuseppe Corrias⁵, Yusuf Erdi¹ and Christopher Kanan²

¹ *Department of Medical Physics, Memorial Sloan Kettering Cancer Center, New York, New York, USA*

² *Chester F. Carlson Center for Imaging Science, Rochester Institute of Technology, Rochester, New York, USA*

³ *Department of Radiology, Memorial Sloan Kettering Cancer Center, New York, New York, USA*

⁴ *Institute of Research and Medical Care (IRCCS) SDN, Naples, Italy*

⁵ *Department of Radiology, University of Cagliari, Cagliari, Italy*

Correspondence*:

Usman Mahmood

mahmoodu@mskcc.org

ABSTRACT

Artificial intelligence (AI) has been successful at solving numerous problems in machine perception. In radiology, AI systems are rapidly evolving and show progress in guiding treatment decisions, diagnosing, localizing disease on medical images, and improving radiologists' efficiency. A critical component to deploying AI in radiology is to gain confidence in a developed system's efficacy and safety. The current gold standard approach is to conduct an analytical validation of performance on a generalization dataset from one or more institutions, followed by a clinical validation study of the system's efficacy during deployment. Clinical validation studies are time-consuming, and best practices dictate limited re-use of analytical validation data, so it is ideal to know ahead of time if a system is likely to fail analytical or clinical validation. In this paper, we describe a series of sanity tests to identify when a system performs well on development data for the wrong reasons. We illustrate the sanity tests' value by designing a deep learning system to classify pancreatic cancer seen in computed tomography scans.

Keywords: Deep learning, Computed Tomography, Bias, Validation, Artificial Intelligence, Spurious Correlations

1 INTRODUCTION

Artificially intelligent (AI) computer-aided diagnostic (CAD) systems have the potential to help radiologists on a multitude of tasks, ranging from tumor classification to improved image reconstruction (Jin et al., 2021; El Naqa et al., 2020; Yala et al., 2019; Antonelli et al., 2019). To deploy medical AI systems, it is essential to validate their performance correctly and to understand their weaknesses before being used on patients (Laghi, 2020; Rudin, 2019; The Lancet, 2018). For AI-based software as a medical device, the gold standard for analytical validation is to assess performance on previously unseen independent datasets (Bluemke et al., 2020; Soffer et al., 2019; Kim et al., 2019; El Naqa et al., 2018), followed by a clinical validation study. Both steps pose challenges for medical AI. First, it is challenging to collect large cohorts of high-quality and diverse medical imaging data sets that are acquired in a consistent manner (Recht et al., 2020; Parmar et al., 2018). Second, both steps are time-consuming, and best practices dictate

limited re-use of analytical validation data. The cost of failing the validation process could prohibit further development of particular applications.

One reason AI systems fail to generalize is that they learn to infer spurious correlations or covariates that can reliably form decision rules that perform well on standard benchmarks (Geirhos et al., 2020). For example, an AI system successfully trained to detect pneumonia from 2D Chest X-rays gathered from multiple institutions, but it failed to generalize when images from new hospitals outside of the training and assessment set were used to evaluate the system (Zech et al., 2018). The investigators found that the system had unexpectedly learned to identify metal tokens seen on the training and assessment images (Zech et al., 2018). In hindsight, the tokens were obvious spurious correlators, but in other cases, the covariates can be less obvious (Geirhos et al., 2020). For example, subtle image characteristics that may be unrelated to the target object, such as high-frequency patterns (Jo and Bengio, 2017; Kafle et al., 2019; Ilyas et al., 2019), object texture (Geirhos et al., 2019; Baker et al., 2018), or intangible attributes of objects are known to cause AI systems to form decision rules that may not generalize (Sinz et al., 2019; Geirhos et al., 2020). Current research has focused on explaining or interpreting AI decisions using various visualization techniques (Reyes et al., 2020), but these do not necessarily imply that a system will generalize (Adebayo et al., 2018; Kim et al., 2018; Ghorbani et al., 2019; Lakkaraju and Bastani, 2020).

Addressing system failures before clinical deployment is critical to ensure that medical AI applications are safe and effective. Identifying systems that are right for the wrong reasons during the development stages can expedite development by not wasting valuable validation data from multiple institutions or conducting doomed clinical validation studies.

The standard approach used to identify system failures involves testing with held-out development or generalization test datasets (Park and Han, 2018). However, development test sets are subsets of the training data, and their primary value lies in identifying systematic errors or bugs within the AI algorithm. Generalization test data are independent of the development data (i.e., their joint probability distribution of inputs and labels differ from training and development test data) (Teney et al., 2020). The generalization data's value is to assess how well a trained model may adapt to previously unseen data. However, neither type of test is sufficiently robust enough to declare when an AI system is ready for the clinic.

We provide a set of sanity tests that can demonstrate if a trained system is right for the wrong reasons. We developed a weakly supervised deep learning system for classifying pancreatic cancer from clinical computed tomography (CT) scans to illustrate their use. Our main contributions are:

1. We provide a set of sanity tests to determine if a system is making predictions using spurious correlations in the data.
2. We describe a system for using deep learning with CT images to detect pancreatic cancer, and we apply our set of sanity tests to both development and generalization test datasets. We train and assess four unique variants of this system to illustrate the pipeline and demonstrate that the system looks as if it performs well in many scenarios, but it is predicting using spurious correlations.
3. We illustrate how to use a method to generate noise images from the patients' volumetric CT scans. These can then be used to assess the influence of noise on the AI system's performance.

2 MATERIALS AND METHODS

2.1 Sanity Tests for AI Systems

There are various testing procedures employed in software engineering to determine if a system is working correctly, such as smoke and sanity tests (Gupta and Saxena, 2013). Smoke tests evaluate the

critical functionality of a system before conducting additional tests. In AI, this is analogous to reaching an acceptable level of performance on the development test data, which matches the training data's distribution. Development test data is typically a random sample of the training data (e.g., 30% test and 70% train). The stopping point for many AI projects is when acceptable performance is achieved on the development test set, but in software engineering, the next step is to conduct 'sanity tests' that indicate if a system produces obvious false results. If the sanity tests fail, further development is done before conducting more time-consuming and rigorous tests, which for AI systems used in medical applications could correspond to analytical and clinical validation studies. For AI systems, sanity tests would identify if a system is achieving good results on the development test set for the wrong reasons (e.g., covariates or spurious correlations) and will therefore fail in other environments or on other datasets.

Sanity tests are occasionally used to identify if a system is unlikely to generalize (Adebayo et al., 2018; Winkler et al., 2019; Oakden-Rayner et al., 2020). However, the tests are often designed to evaluate literature methods instead of being used as a crucial development tool. For example, Shamir et al. critiques the methods by which face datasets were designed and evaluated by showing that commonly used face recognition datasets were classified correctly even when no face, hair, or clothing features appeared in the training and testing datasets (Shamir, 2008). As another example, in response to a report suggesting AI systems could diagnose skin cancer at the level of dermatologists (Esteva et al., 2017), Winkler et al. evaluated the limits of the claim by testing a trained AI system using dermoscopic images where the covariate's, hand-drawn skin markings, were first present and then absent from pictures of the skin cancer. They observed that when skin markings were present, the probability that the AI system classified images as having skin cancer increased significantly. With the markings removed, the probability decreased, which led them to conclude that the AI system associated the markings with cancer instead of the actual pathology (Winkler et al., 2019).

For AI-based medical devices, conducting sanity tests can prevent needless harm to the patient and save a considerable resources. However, without sufficiently large, well-annotated datasets, performing analytical validation to determine the root causes that drive AI systems to fail before deployment remains a challenge (Willeminck et al., 2020). Moreover, after independent testing data is gathered, regulatory organizations advise that the data be used a limited number of times to prevent over-fitting (Petrick et al., 2013). For example, the United States Food and Drug Administration "discourages repeated use of test data in the evaluation" of CAD systems (US Food and Drug Administration, 2020). Clinical validation of deployed systems is likewise time-consuming to organize and often costly.

We propose a series of sanity tests to identify if an AI system may fail during the development phases and before conducting more extensive generalization tests. We also describe how the tests are used with a case study to detect pancreatic cancer from weakly labeled CT scans. The tests are as follows:

- **Train and test with the target-present and absent.** If an AI system is trained to distinguish between normal and abnormal diagnostic features (e.g., organ with cancer shown in Fig. 1a), then it should fail when that target is removed from the development test data (e.g., Fig. 1b). If the system still works effectively after removing the target from testing data, then that indicates it is confounded. In our case study, this corresponds to removing the pancreas from normal scans and pancreas with tumor from abnormal scans using a segmentation mask, as shown in Fig. 1c. We removed the whole pancreas because the pancreatic tumor often distorts the contours of the surrounding anatomy (Galvin et al., 2011).

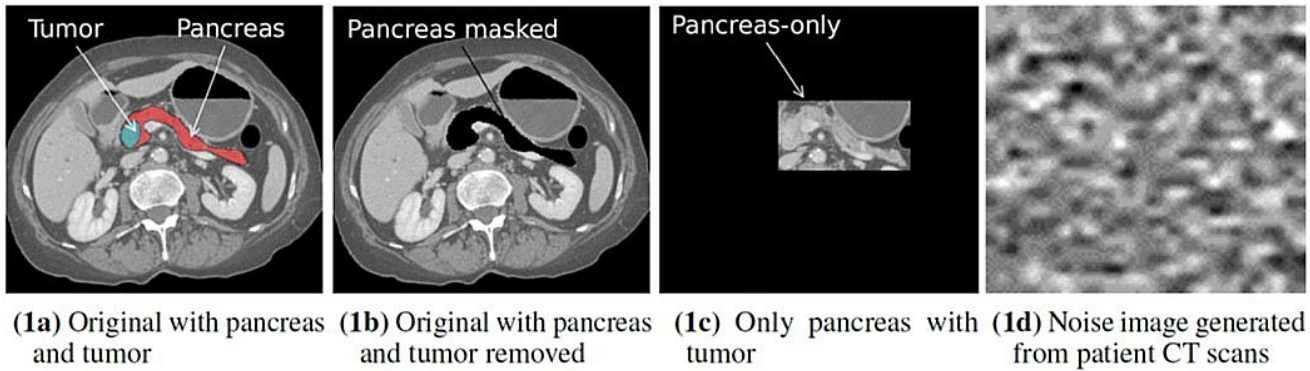


Figure 1. A sample cross sectional axial slice from a patient CT scan processed into the different input formats that were used for the sanity tests. The AI system is trained using each of these input format scenarios and then tested on all of them. **a)** The original image with the pancreas and tumor present. **b)** The original image with the pancreas and tumor removed. **c)** The anatomy surrounding the pancreas is cropped and only the pancreas and tumor remain. **d)** Noise image generated from the patient CT scans. Although this figure shows a single slice, the same processing is applied to all classes, slices and patients in the datasets. A system that is trained to identify the target organ or disease should achieve chance performance when tested with scans where the target or disease is removed.

- **Train and test the system with background patches or noise images.** Background patches consist of non-target regions of the image. Noise images can be generated from the volumetric CT scans in the development and generalization datasets. Both can determine if the different classes can be discriminated based on features unrelated to the target objects (Shamir, 2008). If classes are discriminated against with high confidence using the noise image types, then the system is confounded, and it is using features of the image acquisition process to delineate classes. An example noise image generated from the patient CT scans is shown in Fig. 1d.
- **Test with different regions of interests (ROIs).** Training and testing AI systems on precisely outlined segments of images does not reflect real-world usage. Medical centers, private practices, or institutes where AI is deployed may not have the resources or expertise to precisely outline the anatomical area (Price II, 2019). Furthermore, similar to radiologists, AI systems may have to parse through anatomy they have never encountered during training. Therefore, it is desirable to ensure that when systems are trained on a select portion of images, as shown in Fig. 1c, they can generalize to the original image shown in Fig. 1a.

These sanity tests can be conducted solely using the development dataset, but ideally they would also be used in conjunction with another generalization dataset. They require four input formats, as shown in Fig. 1, to be generated from the same development dataset.

2.2 Datasets

Institutional review board approval was obtained for this Health Insurance Portability and Accountability Act-compliant retrospective study. The requirement for informed consent was waived. The case study is designed as a binary classification problem with the aim of identifying patients who have pancreatic cancer versus those who do not from the provided CT scans. We distinguish between the development dataset used for training, tuning and testing, and the generalization test data used to validate the efficacy of the system.

Development Data. The development dataset consisted of patient CT scans collected from two open-access repositories where detailed annotations were available. The normal pancreas CT scans were obtained

Table 1. Scan parameters and patient-specific characteristics for development and generalization data.

| | Development Data: Train, Tune, & Test | | | Generalization Data |
|--|---------------------------------------|--|-------------------------|---------------------|
| | TCIA - Pancreas CT | Medical Image Segmentation Decathlon (MSD) | | |
| Annotated | Yes | Yes | No | |
| CT Vendor | Phillips and Siemens | General Electric | General Electric | |
| CT Model | ** | LS16 or HD750 | HD750 | |
| Total # of Patients | 82 (27 female/55 male) | 281* | 116 (61 female/55 male) | |
| # used to train | 58 | 60 | NA | |
| # used to tune | 15 | 14 | NA | |
| # used to test | 9 | 8 | 116 | |
| Dataset Information: | | | | |
| Average age (min to max) | 46.8 (18 to 76) | ** | 63 (18 to 90) | |
| Scan start time after contrast administration | ~70s | 80 to 85s | ~40s | |
| Avg. # of total slices (min/max) | 256 (181 to 466) | 95 (37 to 751) | 186 (102 to 278) | |
| Avg. # of slices consisting of only pancreas (min/max) | 85 (45 to 144) | 30 (11 to 147) | NA | |
| Scan parameters: | | | | |
| Tube potential (kVp) | 120 | 120 | 70 keV (80/140 kVp) | |
| Slice thickness (mm) | 1.5 - 2.5 | 2.5 | 2.5 | |
| Pixel dimensions (mm) | 0.664 to 0.977 | 0.606 to 0.977 | 0.547 to 0.976 | |
| Tube current modulation index | ** | Noise Index: 14 (HD750) / 12.5 (LS16) | NA | |
| Tube current (mA) min to max range | ** | 220–380 mA | 260-600 | |
| Rotation time (s) | ** | 0.7 (HD750) / 0.8 (LS16) | 0.7 (HD750) | |
| Pitch | ** | 0.984 (HD750) / 1.375 (LS16) | 0.984 (HD750) | |
| Reconstruction algorithm | ** | ** | ***FBP/ASiR 20% | |
| Reconstruction kernel | ** | ** | Standard | |
| Iterative reconstruction strength | ** | ** | 20% | |
| # of data channels | ** | ** | 64 | |
| Size of a single data channel (mm) | ** | ** | 0.625 | |
| Bowtie filter | ** | ** | Large Body | |
| CT scan series released or used | Axial portal venous phase | Axial portal venous phase | Axial arterial phase | |

*A subset of the MSD dataset was randomly selected to train the model

**Not available in accompanied report or DICOM header

***FBP - Filtered Back Projection, ASiR - Adaptive Statistical Iterative Reconstruction

****LS16: LightSpeed16, HD750: Discovery High Definition 750

from The Cancer Imaging Archive Normal (TCIA) Pancreas Dataset with 82 contrast-enhanced abdominal CT scans (Roth et al., 2016). Seventeen patients from the TCIA dataset were reported to be healthy kidney donors. The remaining patients were selected because they had no major abdominal pathology or pancreatic lesions (Roth et al., 2016). The abnormal pancreas CT scans were obtained from the Medical Image Segmentation Decathlon (MSD) dataset, consisting of abdominal CT scans from 281 patients. The MSD dataset contains patients who presented with intraductal mucinous neoplasms, pancreatic neuroendocrine tumors, or pancreatic ductal adenocarcinoma (Simpson et al., 2019). They were originally used to predict disease-free survival or assess high-risk intraductal papillary mucinous neoplasms seen on the CT scans (Simpson et al., 2019). We randomly selected 82 cases from the MSD dataset to match the TCIA dataset size to avoid class-imbalance issues. The development data were randomly split into a training (58 normal, 60 cancer), tuning (15 normal, 14 cancer), and held-out test (9 normal, 8 cancer) set. To ensure the number of positive and negative samples were balanced in each split, we used stratified 5-fold cross-validation for training. Table 1 shows the patient demographics and scanning parameters provided for each dataset.

Generalization Data: Dual Energy CT (DECT). The generalization data consists of 116 patients (58 without PC, 58 with PC) who received routine DECT scans between June 2015 to December 2017 (see Table 1). The patients without pancreatic cancer received DECT CT Urography (CTU) exams and were selected based on the statement of a negative or unremarkable pancreas and liver in the original radiologist report. Those with cancer were selected if they had undergone a DECT arterial phase CT scan and were histologically confirmed to have pancreatic cancer. All patients were scanned on a 64 slice CT scanner (Discovery CT750 HD, GE Healthcare, Milwaukee, WI, U.S.) with rapid switching DECT following the administration of 150 mL of iodinated contrast (Iohexol 300 mgI/mL, Omnipaque 300, GE Healthcare,

Cork, Ireland), at 4.0 mL/s. The scan parameters are displayed in Table 1. With DECT, multiple image types can be generated, such as virtual monochromatic images (VMI) that depict the anatomy and physiology from the viewpoint of a monochromatic x-ray source (Hsieh, 2003). The VMI scans can be reconstructed at energies ranging from 40 to 140 keV. For this study, all scans were reconstructed at 70 keV because of its use in the clinic. The images were generated using the GSI MD Analysis software available on Advantage Workstation Volume Share 7 (GE Healthcare). Those patients who had a history of surgery and liver abnormalities were excluded from the test set, as were any patients who had metal adjacent to the pancreas or visible artifacts on the scans. This dataset was not used during the training or tuning stages.

2.3 AI System - CTNet

The prediction system is dubbed CTNet. It is designed to map a 3D CT scan to a probability estimate that indicates if pancreatic cancer is present or not. CTNet closely resembles systems in literature that use ImageNet pre-trained convolutional neural networks (CNNs) on radiology scans (Draeos et al., 2021; Raghu et al., 2019; Winkler et al., 2019; Bien et al., 2018; Esteva et al., 2017; Liu et al., 2017; Paul et al., 2016). The model architecture is shown in Fig. 2.

Given a total set of s slices in a scan, where each individual slice t is a 299×299 image, an ImageNet pre-trained Inception v4 CNN was used to extract an embedding $\mathbf{h}_t \in \mathbb{R}^d$ from each slice. The embeddings were extracted from the penultimate layer, which renders a $d = 1536$ dimensional feature vector for each image (Szegedy et al., 2017). Because Inception v4 is designed to take as input a $299 \times 299 \times 3$ RGB image, we replicated each slice to create faux RGB images. Following others (Van Ginneken et al., 2015), the CNN was not fine-tuned for CT data.

After extracting the embeddings from all scan slices, they are fed into a neural network that makes the final prediction, which is given by

$$P(\text{Cancer} = 1 | \mathbf{h}_1, \mathbf{h}_2, \dots, \mathbf{h}_s) = \sigma \left(b + \frac{1}{s} \mathbf{w}^T \sum_{t=1}^s \text{ReLU}(\mathbf{U} \mathbf{h}_t + \mathbf{a}) \right), \quad (1)$$

where $\sigma(\cdot)$ denotes the logistic sigmoid activation function, $b \in \mathbb{R}$ is the output layer bias, $\mathbf{w} \in \mathbb{R}^{20}$ is the output layer's weight vector, $\mathbf{U} \in \mathbb{R}^{20 \times 1536}$ is the hidden layer weight matrix, $\mathbf{a} \in \mathbb{R}^{20}$ is the hidden layer bias, and ReLU is the rectified linear unit activation function. In preliminary studies, we found that using 20 hidden units sufficed to achieve strong performance. If the predicted probability was above 0.5, then the patient was classified as positive for pancreatic cancer.

The model was trained using the binary cross-entropy loss function with a mini-batch size of 1. The weights were initialized using the Kaiming method. For all systems trained in this study, we used the Adam optimizer with (Kingma and Ba, 2015) a base learning rate of $1e^{-4}$, L_2 weight decay of $1e^{-6}$, and bias correction terms, $\beta_1 = 0.9$ and $\beta_2 = 0.999$. The learning rate was reduced by a factor of 2 over the course of training when the validation loss had stopped improving. The system was trained for 100 epochs. Since our training dataset was balanced, we did not scale the loss for any particular class's prevalence. During training, no data augmentation techniques were applied. The model was implemented in Python 3.8 with PyTorch 1.6.0 on a computer with a 12 GB NVIDIA Titan V GPU.

2.4 Scan Preprocessing

Since the voxel size varied from patient to patient, the CT scans were first resampled to an isotropic resolution of $1.0 \times 1.0 \times 1.0$ mm using SINC interpolation. They were then resized to a height and width of 299×299 pixels using bilinear interpolation, which is the original input image size used to train the

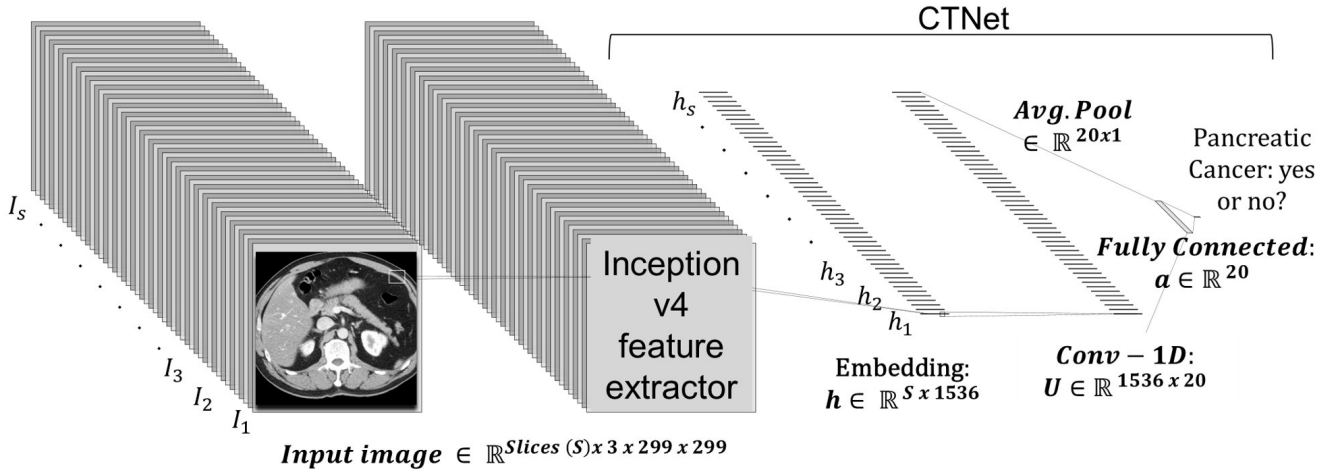


Figure 2. CTNet architecture. CTNet takes as input a volumetric CT scan and outputs a classification prediction. Features are extracted from each slice of the CT scan by the Inception v4 network. The output feature vector is then reduced in dimension with a single convolutional layer, followed by an adaptive average pooling operation applied over the number slices. The resulting vector is fed into a fully connected layer, which has a single output.

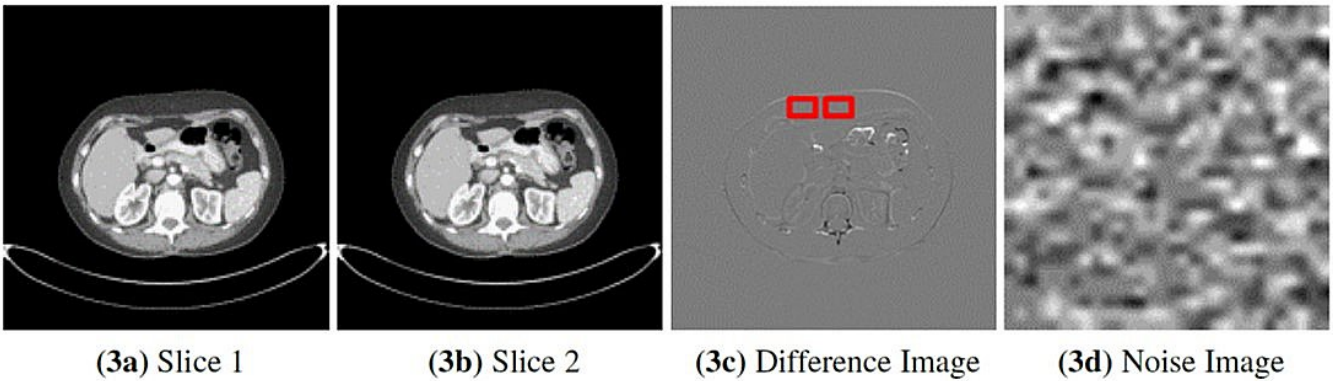


Figure 3. Method to obtain noise maps from sequentially acquired images. Two sequential slice images are subtracted from each other (a and b). c) Difference image resulting from subtraction showing the sliding 30×30 pixel window used to extract uniform patches. d) All patches were averaged to generate a single noise image.

Inception v4 network. The voxel Hounsfield unit (HU) value was clipped to be between $\pm 300HU$ and normalized to have zero mean and unit variance (i.e., $[0, 1]$). Normalization was performed by subtracting the mean and dividing by the standard deviation computed from the training dataset. This processing was applied to both the development and generalization datasets.

2.5 Noise Image Generation

The noise images are used to determine if the institutional scanning practices or noise characteristics of the imaging systems confound the classification results. A key characteristic of the image is that they must be uniform and devoid of any perceptible patterns. We generated noise images from each patient’s CT scan using an approach similar to (Christianson et al., 2015; Tian and Samei, 2016), and as shown in Fig. 4. For a scan with s sequential slices, where each slice t is an image $I_t \in \mathbb{R}^{299 \times 299}$, we subtract adjacent slices to produce $s - 1$ difference images D_I , where $D_I = I_t - I_{t-1}$ and $1 \leq t < s$. The subtraction process eliminates most of the anatomical features seen in the scan. We then apply a Sobel

edge enhancing filter to each D_I to identify and remove any remaining anatomical patterns. Then we loop through each D_I to extract non-overlapping patches of size 30×30 pixels. The patch size was selected to minimize the impact of the non-uniformity of the CT HU values within the region of interest (e.g., due to streaking or beam hardening artifacts) (Tian and Samei, 2016). However, patches of transitional boundary areas (i.e., interface between different tissue types) consisted of discernible patterns that could be spuriously correlated with the class labels. Consequently, to identify and exclude boundary patches, we generated and analyzed each patch’s histogram. First-order statistical measures, such as skewness, kurtosis, and the standard deviation and the number of peaks within the histogram were used to identify and exclude boundary patches. Histograms with a skewness value within ± 0.1 , kurtosis of 3.0 ± 0.5 , a standard deviation less than 16, and those with a single peak were included. Published descriptions of the noise image generation method do not provide choices for each of the parameters, so we chose them via visual inspection to eliminate transition areas or edges. The patches that met the criteria were then averaged together to create a single noise image representation of size 30×30 for the D_I , as shown in Fig. 3. Finally, the $s - 1$ noise images for the patient were upsampled using SINC interpolation to a dimension of 299×299 .

2.6 Experiments

To employ the sanity tests, we processed four representations or input formats of the training, tuning, and held out development test sets. Representative images are shown in Fig. 1. For the first format, termed pancreas-only (Fig. 1c), we used the provided annotations to crop out the area surrounding the normal pancreas and the pancreas with tumor from each scan so that only the target areas remained. The second format, shown in Fig. 1a, consisted of the original uncropped scans. For the third format, the annotations were used to remove the pancreas and pancreas with tumor from the original uncropped scans, Fig. 1b. The fourth format consisted of the noise images. We trained four systems, one for each input format, and tested each of them with the held-out test sets of the other formats. Since annotations were not available for the generalization test set, we generated two formats: 1) the original uncropped images and 2) the noise images. We performed stratified 5-fold cross-validation with the same division of scans across the four systems. For this study, we consider the baseline against which all results are compared to be the system trained with the pancreas-only scans shown in Fig. 1c, as it should be the representation that maximizes the signal to noise ratio.

2.7 Statistical Analysis

Each system’s classification performance was assessed using the area under the receiver operator characteristic curve (AUC). We report the average AUC and corresponding 95% confidence interval (CI) across cross-validation runs. An average AUC score of 1.0 represents perfect classification performance. The average AUC across runs and the corresponding confidence intervals were determined using R (Rstudio version 3.6.2) with the package `cvAUC` for cross-validated AUC (LeDell et al., 2015). In addition to confidence intervals, statistically significant differences between test runs was confirmed with the DeLong test statistic for AUCs (DeLong et al., 1988). The level of significance was set at $P \leq .05$. Table 2 provides an overview of how the sanity tests should be interpreted and implemented in practice.

3 RESULTS

Our main results are shown in Fig. 4. Each row corresponds to the cross-validated AUC obtained when training on one input format and testing on all other formats. The diagonal elements for the development tests correspond to training and testing on the same input format (i.e., self-tests), while the others represent AUC scores from training on one variant and testing on the another (i.e., non-self tests). We expect a system trained on one format to perform the best on test data processed in an identical manner, which is consistent

Table 2. The proposed sanity tests to assess the reliability of medical AI systems.

| Sanity Test | Implications of Failing the Test | Does CTNet Pass the Test? |
|--|---|---------------------------|
| Train & test with and without the target: The system should achieve an AUC of around 0.5 when tested without the target in test images. | Images contain spurious covariates that can be exploited by the model. | X |
| Train & test using noise images: The system should achieve an AUC of around 0.5 on test data. | Classification performance cannot be attributed to recognition of the target (i.e., covariates contribute to the learned classification decision rule). | X |
| Test system with different sized ROIs: The additional or reduced context should not alter the performance. | The system cannot decorrelate features of the target from its co-occurring context (i.e., Contextual Bias (Singh et al., 2020)). | X |

with our results. The system trained with the pancreas-only images achieved an AUC of 0.82 (95% CI: 0.73 - 0.92) on its self-test set. If the system was considered to pass the sanity tests, we would expect it to have the highest AUC across all input formats. However, instead, it is the lowest among the self-tests. Its performance is significantly lower ($P < .001$) than systems trained on the original scans, with and without the pancreas present, 0.95 AUC (95% CI: 0.89 - 1.0) and 0.97 AUC (95% CI: 0.93 - 1.0), respectively. The noise only system achieved the highest AUC of 0.98 (95% CI: 0.96 - 1.0) on its self test set.

Our results indicate that this dataset with CTNet fails all of the sanity tests. The self-tests for the noise images and the no pancreas format achieved the highest AUCs rather than being near a score of 0.5. This result on the development data is confirmed on the generalization tests where these system’s performances are significantly lower lower than on the development data self-tests ($P < .001$).

4 DISCUSSION

Identifying covariates that cause unintended generalization or those that cause machines to fail unexpectedly in deployment remains a challenge across deep learning applications. We described sanity tests that could reveal if covariates drive classification decision-making and tested them with a case study designed to classify pancreatic cancer from CT scans. Failing these sanity tests provides an early indicator of potential biases being responsible for the observed performance and that further in the development process, a system will unintentionally generalize or have much lower performance when deployed. These were reflected in our generalization experiment results. We argue that others should routinely use these tests in publications. For industry, these tests could save time and money. Failing them indicates that the target objects’ attributes are not being used by the systems undergoing analytical and clinical validation studies. Hence, as we show, relying only on conventional testing strategies with development data will not provide adequate assurances of generalization. Our sanity tests can be used with development data as long as ROIs are available or a background noise image can be generated. While we focused on binary classification, the sanity tests apply to the multi-class classification and regression problems, with appropriate statistical analysis modifications.

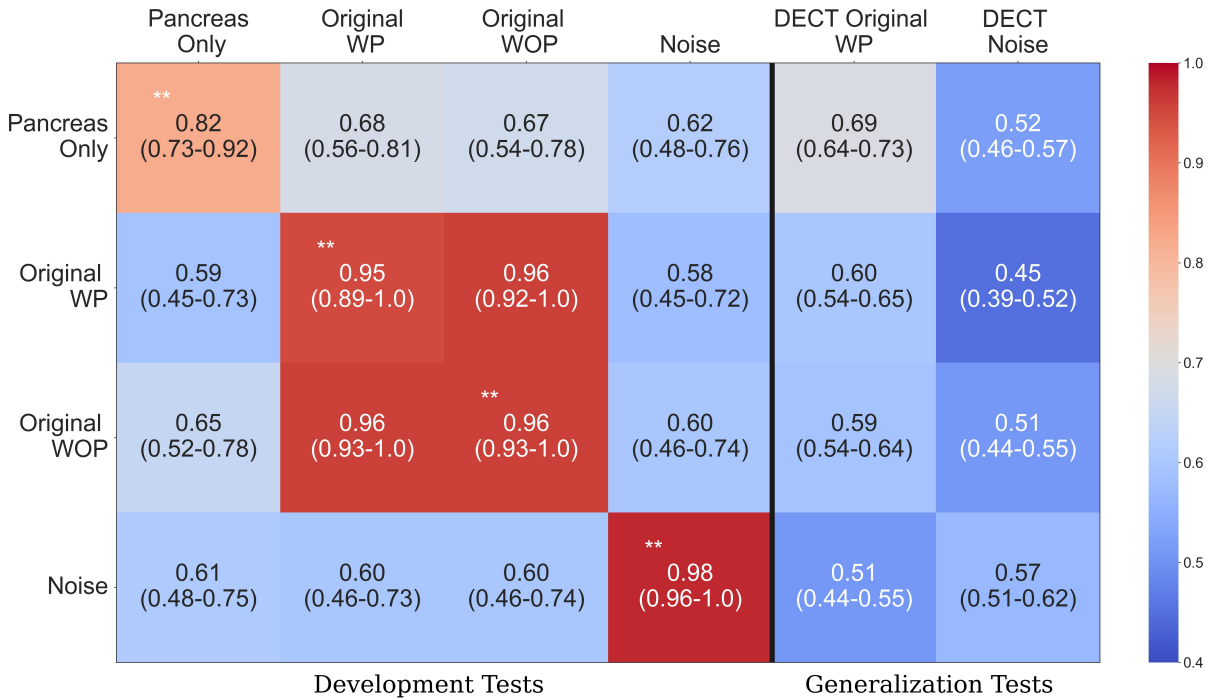


Figure 4. AUC heatmap across models for each input format type. Each row indicates the cross-validated mean AUC with 95% confidence intervals for the systems trained with a given input format and assessed across all input format variants on the development dataset (first four columns) and generalization dataset (last two columns). The diagonal elements on the development tests correspond to training and testing with the same input format. The last two columns show mean AUC on the generalization dataset with the original and the noise formats. Red indicates the highest AUC values, while light blue indicates the lowest AUC values. The results indicate that the system correctly classifies patients using spurious correlations, instead of features specific to pancreatic cancer. **Test images processed identically to the data used for training that model. DECT = Dual Energy CT.

We did not attempt to use techniques to mitigate the impact of spurious correlations. These include adversarial regularization (Ramakrishnan et al., 2018; Zhang et al., 2018; Ilyas et al., 2019), model ensembling (Cadène et al., 2019; Clark et al., 2019), invariant risk minimization (Arjovsky et al., 2019; Choe et al., 2020) and methods that encourage grounding on causal factors instead of spurious correlations (Selvaraju et al., 2019; Qi et al., 2020; Agarwal et al., 2020; Castro et al., 2020). However, as shown by Shrestha et al. (Shrestha et al., 2020), methods that were thought to overcome spurious correlations were behaving as regularizers instead of overcoming the issues that stemmed from the covariates. Our sanity tests could be used with these mitigation methods to measure their true impact, in that we would expect them to only be able to provide significant benefit when the target is present.

There are some limitations to this study. As with most AI studies involving medical image analysis, we trained and tested with a small dataset. Results stemming from small-data may not always transfer to scenarios where larger datasets are used to train systems, but this is in part why sanity tests when using smaller datasets are critical since it is likely easier for spurious correlations to impact them. Our sanity tests help reveal when an AI model predicts the right answer for the wrong reasons and will therefore have a large gap between development and external generalization tests. A complementary approach uses visualization methods to understand if a system is not looking at the target to perform its classification.

In conclusion, we demonstrated how our proposed sanity tests could identify spurious confounds early, using development data solely. While the methods are simple, we argue that sanity tests similar to these

should be performed wherever possible, especially with smaller datasets, and if no external dataset is available. Otherwise, study results can be very misleading and fail to generalize on other datasets. In safety-critical AI domains, such as healthcare, sanity tests could prevent harm to patients, and they could better prepare novel medical AI systems for regulatory approval. We present a workflow and practical sanity tests that can reliably reveal error-prone systems before influencing real-world decision-making.

CONFLICT OF INTEREST STATEMENT

CK was employed at Paige, a commercial company, during the preparation of this manuscript. This company played no role in the sponsorship, design, data collection and analysis, decision to publish, or preparation of the manuscript. The other authors declare that the research was conducted in the absence of any commercial or financial relationships that could be construed as a potential conflict of interest.

AUTHOR CONTRIBUTIONS

UM and CK conceived the study. UM implemented the algorithms and carried out the experiments. UM, CK, and RS wrote the paper. DB, LM, GC, and YE helped gather the data, provided advice, and reviewed the manuscript.

FUNDING

This research was funded in part through the National Institutes of Health/National Cancer Institute Cancer Center support grant P30 CA008748 as well as by NSF award #1909696.

DATA AVAILABILITY STATEMENT

The datasets used to train for this study can be found in the TCIA Pancreas CT dataset, <https://wiki.cancerimagingarchive.net/display/Public/Pancreas-CT>, and in the Medical Image Segmentation Decathlon Pancreas Dataset, <http://medicaldecathlon.com/>.

REFERENCES

- Adebayo, J., Gilmer, J., Muelly, M., Goodfellow, I. J., Hardt, M., and Kim, B. (2018). Sanity checks for saliency maps. In *Advances in Neural Information Processing Systems 31: Annual Conference on Neural Information Processing Systems 2018, NeurIPS 2018, December 3-8, 2018, Montréal, Canada*, eds. S. Bengio, H. M. Wallach, H. Larochelle, K. Grauman, N. Cesa-Bianchi, and R. Garnett. 9525–9536
- Agarwal, V., Shetty, R., and Fritz, M. (2020). Towards causal VQA: revealing and reducing spurious correlations by invariant and covariant semantic editing. In *2020 IEEE/CVF Conference on Computer Vision and Pattern Recognition, CVPR 2020, Seattle, WA, USA, June 13-19, 2020* (IEEE), 9687–9695. doi:10.1109/CVPR42600.2020.00971
- Antonelli, M., Johnston, E. W., Dikaios, N., Cheung, K. K., Sidhu, H. S., Appayya, M. B., et al. (2019). Machine learning classifiers can predict gleason pattern 4 prostate cancer with greater accuracy than experienced radiologists. *European radiology* 29, 4754–4764. doi:10.1007/s00330-019-06244-2
- Arjovsky, M., Bottou, L., Gulrajani, I., and Lopez-Paz, D. (2019). Invariant risk minimization. *arXiv preprint arXiv:1907.02893*
- Baker, N., Lu, H., Erlikhman, G., and Kellman, P. J. (2018). Deep convolutional networks do not classify based on global object shape. *PLoS computational biology* 14, e1006613. doi:10.1371/journal.pcbi.1006613

- Bien, N., Rajpurkar, P., Ball, R. L., Irvin, J., Park, A., Jones, E., et al. (2018). Deep-learning-assisted diagnosis for knee magnetic resonance imaging: development and retrospective validation of mrnet. *PLoS medicine* 15, e1002699. doi:10.1371/journal.pmed.1002699
- Bluemke, D. A., Moy, L., Bredella, M. A., Ertl-Wagner, B. B., Fowler, K. J., Goh, V. J., et al. (2020). Assessing radiology research on artificial intelligence: A brief guide for authors, reviewers, and readers—from the radiology editorial board. *Radiology* 294, 487–489. doi:10.1148/radiol.2019192515. PMID: 31891322
- Cadène, R., Dancette, C., Ben-younes, H., Cord, M., and Parikh, D. (2019). Rubi: Reducing unimodal biases for visual question answering. In *Advances in Neural Information Processing Systems 32: Annual Conference on Neural Information Processing Systems 2019, NeurIPS 2019, December 8-14, 2019, Vancouver, BC, Canada*, eds. H. M. Wallach, H. Larochelle, A. Beygelzimer, F. d’Alché-Buc, E. B. Fox, and R. Garnett. 839–850
- Castro, D. C., Walker, I., and Glocker, B. (2020). Causality matters in medical imaging. *Nature Communications* 11, 1–10. doi:10.1038/s41467-020-17478-w
- Choe, Y. J., Ham, J., and Park, K. (2020). An empirical study of invariant risk minimization. *arXiv preprint arXiv:2004.05007*
- Christianson, O., Winslow, J., Frush, D. P., and Samei, E. (2015). Automated technique to measure noise in clinical ct examinations. *American Journal of Roentgenology* 205, W93–W99. doi:10.2214/AJR.14.13613
- Clark, C., Yatskar, M., and Zettlemoyer, L. (2019). Don’t take the easy way out: Ensemble based methods for avoiding known dataset biases. In *Proceedings of the 2019 Conference on Empirical Methods in Natural Language Processing and the 9th International Joint Conference on Natural Language Processing (EMNLP-IJCNLP)* (Hong Kong, China: Association for Computational Linguistics), 4069–4082. doi:10.18653/v1/D19-1418
- DeLong, E. R., DeLong, D. M., and Clarke-Pearson, D. L. (1988). Comparing the areas under two or more correlated receiver operating characteristic curves: a nonparametric approach. *Biometrics* , 837–845doi:10.2307/2531595
- Draeos, R. L., Dov, D., Mazurowski, M. A., Lo, J. Y., Henao, R., Rubin, G. D., et al. (2021). Machine-learning-based multiple abnormality prediction with large-scale chest computed tomography volumes. *Medical Image Analysis* 67, 101857. doi:10.1016/j.media.2020.101857
- El Naqa, I., Haider, M. A., Giger, M. L., and Ten Haken, R. K. (2020). Artificial intelligence: reshaping the practice of radiological sciences in the 21st century. *The British Journal of Radiology* 93, 20190855. doi:10.1259/bjr.20190855
- El Naqa, I., Ruan, D., Valdes, G., Dekker, A., McNutt, T., Ge, Y., et al. (2018). Machine learning and modeling: Data, validation, communication challenges. *Medical physics* 45, e834–e840. doi:10.1002/mp.12811
- Esteva, A., Kuprel, B., Novoa, R. A., Ko, J., Swetter, S. M., Blau, H. M., et al. (2017). Dermatologist-level classification of skin cancer with deep neural networks. *nature* 542, 115–118. doi:https://doi.org/10.1038/nature21056
- Galvin, A., Sutherland, T., and Little, A. F. (2011). Part 1: Ct characterisation of pancreatic neoplasms: a pictorial essay. *Insights into imaging* 2, 379–388. doi:10.1007/s13244-011-0102-7
- Geirhos, R., Jacobsen, J.-H., Michaelis, C., Zemel, R., Brendel, W., Bethge, M., et al. (2020). Shortcut learning in deep neural networks. *Nature Machine Intelligence* 2, 665–673. doi:10.1038/s42256-020-00257-z

- Geirhos, R., Rubisch, P., Michaelis, C., Bethge, M., Wichmann, F. A., and Brendel, W. (2019). Imagenet-trained cnns are biased towards texture; increasing shape bias improves accuracy and robustness. In *7th International Conference on Learning Representations, ICLR 2019, New Orleans, LA, USA, May 6-9, 2019* (OpenReview.net)
- Ghorbani, A., Abid, A., and Zou, J. Y. (2019). Interpretation of neural networks is fragile. In *The Thirty-Third AAAI Conference on Artificial Intelligence, AAAI 2019, The Thirty-First Innovative Applications of Artificial Intelligence Conference, IAAI 2019, The Ninth AAAI Symposium on Educational Advances in Artificial Intelligence, EAAI 2019, Honolulu, Hawaii, USA, January 27 - February 1, 2019* (AAAI Press), 3681–3688. doi:10.1609/aaai.v33i01.33013681
- Gupta, V. and Saxena, V. (2013). Software testing: Smoke and sanity. *International Journal of Engineering Research & Technology* 2, 1674–1678
- Hsieh, J. (2003). *Computed tomography: principles, design, artifacts, and recent advances*, vol. 114 (SPIE press)
- Ilyas, A., Santurkar, S., Tsipras, D., Engstrom, L., Tran, B., and Madry, A. (2019). Adversarial examples are not bugs, they are features. In *Advances in Neural Information Processing Systems 32: Annual Conference on Neural Information Processing Systems 2019, NeurIPS 2019, December 8-14, 2019, Vancouver, BC, Canada*, eds. H. M. Wallach, H. Larochelle, A. Beygelzimer, F. d’Alché-Buc, E. B. Fox, and R. Garnett. 125–136
- Jin, D., Harrison, A. P., Zhang, L., Yan, K., Wang, Y., Cai, J., et al. (2021). Chapter 14 - artificial intelligence in radiology. In *Artificial Intelligence in Medicine*, eds. L. Xing, M. L. Giger, and J. K. Min (Academic Press). 265–289. doi:https://doi.org/10.1016/B978-0-12-821259-2.00014-4
- Jo, J. and Bengio, Y. (2017). Measuring the tendency of cnns to learn surface statistical regularities. *arXiv preprint arXiv:1711.11561* doi:https://arxiv.org/abs/1711.11561
- Kafle, K., Shrestha, R., and Kanan, C. (2019). Challenges and prospects in vision and language research. *Frontiers in Artificial Intelligence* 2, 28. doi:10.3389/frai.2019.00028
- Kim, B., Wattenberg, M., Gilmer, J., Cai, C. J., Wexler, J., Viégas, F. B., et al. (2018). Interpretability beyond feature attribution: Quantitative testing with concept activation vectors (TCAV). In *Proceedings of the 35th International Conference on Machine Learning, ICML 2018, Stockholmsmässan, Stockholm, Sweden, July 10-15, 2018*, eds. J. G. Dy and A. Krause (PMLR), vol. 80 of *Proceedings of Machine Learning Research*, 2673–2682
- Kim, D. W., Jang, H. Y., Kim, K. W., Shin, Y., and Park, S. H. (2019). Design characteristics of studies reporting the performance of artificial intelligence algorithms for diagnostic analysis of medical images: results from recently published papers. *Korean journal of radiology* 20, 405–410. doi:10.3348/kjr.2019.0025
- Kingma, D. P. and Ba, J. (2015). Adam: A method for stochastic optimization. In *3rd International Conference on Learning Representations, ICLR 2015, San Diego, CA, USA, May 7-9, 2015, Conference Track Proceedings*, eds. Y. Bengio and Y. LeCun
- Laghi, A. (2020). Cautions about radiologic diagnosis of covid-19 infection driven by artificial intelligence. *The Lancet Digital Health* 2, e225. doi:10.1016/S2589-7500(20)30079-0
- Lakkaraju, H. and Bastani, O. (2020). ” how do i fool you?” manipulating user trust via misleading black box explanations. In *Proceedings of the AAAI/ACM Conference on AI, Ethics, and Society*. 79–85. doi:10.1145/3375627.3375833
- LeDell, E., Petersen, M., and van der Laan, M. (2015). Computationally efficient confidence intervals for cross-validated area under the roc curve estimates. *Electronic journal of statistics* 9, 1583. doi:10.1214/15-EJS1035

- Liu, J., Wang, D., Lu, L., Wei, Z., Kim, L., Turkbey, E. B., et al. (2017). Detection and diagnosis of colitis on computed tomography using deep convolutional neural networks. *Medical physics* 44, 4630–4642. doi:10.1002/mp.12399
- Oakden-Rayner, L., Dunnmon, J., Carneiro, G., and Ré, C. (2020). Hidden stratification causes clinically meaningful failures in machine learning for medical imaging. In *Proceedings of the ACM Conference on Health, Inference, and Learning*. 151–159. doi:10.1145/3368555.3384468
- Park, S. H. and Han, K. (2018). Methodologic guide for evaluating clinical performance and effect of artificial intelligence technology for medical diagnosis and prediction. *Radiology* 286, 800–809. doi:10.1148/radiol.2017171920
- Parmar, C., Barry, J. D., Hosny, A., Quackenbush, J., and Aerts, H. J. (2018). Data analysis strategies in medical imaging. *Clinical cancer research* 24, 3492–3499. doi:10.1158/1078-0432.CCR-18-0385
- Paul, R., Hawkins, S. H., Balagurunathan, Y., Schabath, M. B., Gillies, R. J., Hall, L. O., et al. (2016). Deep feature transfer learning in combination with traditional features predicts survival among patients with lung adenocarcinoma. *Tomography* 2, 388. doi:10.18383/j.tom.2016.00211
- Petrick, N., Sahiner, B., Armato III, S. G., Bert, A., Correale, L., Delsanto, S., et al. (2013). Evaluation of computer-aided detection and diagnosis systems a. *Medical physics* 40, 087001. doi:10.1118/1.4816310
- Price II, W. N. (2019). Medical ai and contextual bias. *Harvard Journal of Law & Technology* 33
- Qi, J., Niu, Y., Huang, J., and Zhang, H. (2020). Two causal principles for improving visual dialog. In *2020 IEEE/CVF Conference on Computer Vision and Pattern Recognition, CVPR 2020, Seattle, WA, USA, June 13-19, 2020* (IEEE), 10857–10866. doi:10.1109/CVPR42600.2020.01087
- Raghu, M., Zhang, C., Kleinberg, J. M., and Bengio, S. (2019). Transfusion: Understanding transfer learning for medical imaging. In *Advances in Neural Information Processing Systems 32: Annual Conference on Neural Information Processing Systems 2019, NeurIPS 2019, December 8-14, 2019, Vancouver, BC, Canada*, eds. H. M. Wallach, H. Larochelle, A. Beygelzimer, F. d’Alché-Buc, E. B. Fox, and R. Garnett. 3342–3352
- Ramakrishnan, S., Agrawal, A., and Lee, S. (2018). Overcoming language priors in visual question answering with adversarial regularization. In *Advances in Neural Information Processing Systems 31: Annual Conference on Neural Information Processing Systems 2018, NeurIPS 2018, December 3-8, 2018, Montréal, Canada*, eds. S. Bengio, H. M. Wallach, H. Larochelle, K. Grauman, N. Cesa-Bianchi, and R. Garnett. 1548–1558
- Recht, M. P., Dewey, M., Dreyer, K., Langlotz, C., Niessen, W., Prainsack, B., et al. (2020). Integrating artificial intelligence into the clinical practice of radiology: challenges and recommendations. *European radiology* , 1–9doi:10.1007/s00330-020-06672-5
- Reyes, M., Meier, R., Pereira, S., Silva, C. A., Dahlweid, F.-M., Tengg-Kobligk, H. v., et al. (2020). On the interpretability of artificial intelligence in radiology: Challenges and opportunities. *Radiology: Artificial Intelligence* 2, e190043. doi:10.1148/ryai.2020190043
- [Dataset] Roth, H. R., Farag, A., Turkbey, E., Lu, L., Liu, J., and Summers, R. M. (2016). Data from pancreas-ct. the cancer imaging archive. doi:10.7937/K9/TCIA.2016.tNB1kqBU
- Rudin, C. (2019). Stop explaining black box machine learning models for high stakes decisions and use interpretable models instead. *Nature Machine Intelligence* 1, 206–215. doi:10.1038/s42256-019-0048-x
- Selvaraju, R. R., Lee, S., Shen, Y., Jin, H., Ghosh, S., Heck, L. P., et al. (2019). Taking a HINT: leveraging explanations to make vision and language models more grounded. In *2019 IEEE/CVF International Conference on Computer Vision, ICCV 2019, Seoul, Korea (South), October 27 - November 2, 2019* (IEEE), 2591–2600. doi:10.1109/ICCV.2019.00268

- Shamir, L. (2008). Evaluation of face datasets as tools for assessing the performance of face recognition methods. *International Journal of Computer Vision* 79, 225. doi:10.1007/s11263-008-0143-7
- Shrestha, R., Kafle, K., and Kanan, C. (2020). A negative case analysis of visual grounding methods for VQA. In *Proceedings of the 58th Annual Meeting of the Association for Computational Linguistics* (Online: Association for Computational Linguistics), 8172–8181. doi:10.18653/v1/2020.acl-main.727
- [Dataset] Simpson, A. L., Antonelli, M., Bakas, S., Bilello, M., Farahani, K., van Ginneken, B., et al. (2019). A large annotated medical image dataset for the development and evaluation of segmentation algorithms
- Singh, K. K., Mahajan, D., Grauman, K., Lee, Y. J., Feiszli, M., and Ghadiyaram, D. (2020). Don't judge an object by its context: Learning to overcome contextual bias. In *2020 IEEE/CVF Conference on Computer Vision and Pattern Recognition, CVPR 2020, Seattle, WA, USA, June 13-19, 2020* (IEEE), 11067–11075. doi:10.1109/CVPR42600.2020.01108
- Sinz, F. H., Pitkow, X., Reimer, J., Bethge, M., and Tolias, A. S. (2019). Engineering a less artificial intelligence. *Neuron* 103, 967–979. doi:10.1016/j.neuron.2019.08.034
- Soffer, S., Ben-Cohen, A., Shimon, O., Amitai, M. M., Greenspan, H., and Klang, E. (2019). Convolutional neural networks for radiologic images: a radiologist's guide. *Radiology* 290, 590–606. doi:10.1148/radiol.2018180547
- Szegedy, C., Ioffe, S., Vanhoucke, V., and Alemi, A. A. (2017). Inception-v4, inception-resnet and the impact of residual connections on learning. In *Proceedings of the Thirty-First AAAI Conference on Artificial Intelligence, February 4-9, 2017, San Francisco, California, USA*, eds. S. P. Singh and S. Markovitch (AAAI Press), 4278–4284
- Teney, D., Kafle, K., Shrestha, R., Abbasnejad, E., Kanan, C., and Hengel, A. v. d. (2020). On the value of out-of-distribution testing: An example of goodhart's law. *arXiv preprint arXiv:2005.09241*
- The Lancet (2018). Is digital medicine different? *The Lancet* 392, 95. doi:10.1016/S0140-6736(18)31562-9
- Tian, X. and Samei, E. (2016). Accurate assessment and prediction of noise in clinical ct images. *Medical physics* 43, 475–482. doi:10.1118/1.4938588
- US Food and Drug Administration (2020). Clinical performance assessment: Considerations for computer-assisted detection devices applied to radiology images and radiology device data—premarket approval (pma) and premarket notification [510 (k)] submissions. *Silver Spring (MD/USA):[sn]. Disponible em: j https://www.fda.gov/media/77642/download*
- Van Ginneken, B., Setio, A. A., Jacobs, C., and Ciompi, F. (2015). Off-the-shelf convolutional neural network features for pulmonary nodule detection in computed tomography scans. In *2015 IEEE 12th International symposium on biomedical imaging (ISBI)* (IEEE), 286–289. doi:10.1109/ISBI.2015.7163869
- Willemink, M. J., Koszek, W. A., Hardell, C., Wu, J., Fleischmann, D., Harvey, H., et al. (2020). Preparing medical imaging data for machine learning. *Radiology* 295, 4–15. doi:doi.org/10.1148/radiol.2020192224
- Winkler, J. K., Fink, C., Toberer, F., Enk, A., Deinlein, T., Hofmann-Wellenhof, R., et al. (2019). Association between surgical skin markings in dermoscopic images and diagnostic performance of a deep learning convolutional neural network for melanoma recognition. *JAMA dermatology* 155, 1135–1141. doi:10.1001/jamadermatol.2019.1735
- Yala, A., Lehman, C., Schuster, T., Portnoi, T., and Barzilay, R. (2019). A deep learning mammography-based model for improved breast cancer risk prediction. *Radiology* 292, 60–66. doi:10.1148/radiol.2019182716

- Zech, J. R., Badgeley, M. A., Liu, M., Costa, A. B., Titano, J. J., and Oermann, E. K. (2018). Variable generalization performance of a deep learning model to detect pneumonia in chest radiographs: a cross-sectional study. *PLoS medicine* 15, e1002683. doi:10.1371/journal.pmed.1002683
- Zhang, B. H., Lemoine, B., and Mitchell, M. (2018). Mitigating unwanted biases with adversarial learning. In *Proceedings of the 2018 AAAI/ACM Conference on AI, Ethics, and Society*. 335–340. doi:10.1145/3278721.3278779